IEICE TRANS. COMMUN., VOL.E96–B, NO.6 JUNE 2013

PAPER

Performance Evaluation of Interference-Aware Multi-Cell Beamforming for an Overlapping Cells Environment

Tomoki MURAKAMI[†a)], **Riichi KUDO**[†], **Takeo ICHIKAWA**[†], **Naoki HONMA**[††], *and* **Masato MIZOGUCHI**[†], *Members*

SUMMARY As wireless LAN systems become more widespread, the number of access points (APs) is increasing. A large number of APs cause overlapping cells where nearby cells utilize the same frequency channel. In the overlapping cells, inter-cell interference (ICI) degrades the throughput. This paper proposes an interference-aware multi-cell beamforming (IMB) technique to reduce the throughput degradation in the overlapping cells. The IMB technique improves transmission performance better than conventional multi-cell beamforming based on a decentralized control scheme. The conventional technique mitigates ICI by nullifying all the interference signal space (ISS) by beamforming, but the signal spaces to the user terminal (UT) is also limited because the degree of freedom (DoF) at the AP is limited. On the other hand, the IMB technique increases the signal space to the UT because the DoF at the AP is increased by selecting the ISS by allowing a small amount of ICI. In addition, we introduce a method of selecting the ISS in a decentralized control scheme. In our work, we analyze the interference channel state information (CSI) and evaluate the transmission performance of the IMB technique by using a measured CSI in an actual indoor environment. As a result, we find that the IMB technique becomes more effective as the number of UT antennas in nearby cells increases.

key words: *MIMO, multi-cell beamforming, inter-cell interference (ICI), WLAN, decentralized control scheme*

1. Introduction

Due to rising demand for wireless communication such as that over wireless LAN (WLAN) systems, the number of wireless devices is greatly increasing. The widespread use of WLAN systems results in many closely located access points (APs) and consequently the number of overlapping cells is increasing. Throughput in overlapping cells degrades by inter-cell interference (ICI) because the transmissions must be separated in time domain by carrier sense multiple access/collision avoidance (CSMA/CA). Furthermore, the number of available channels is decreasing because of the increased bandwidth of each channel. In the IEEE802.11n standard, the bandwidth is extended from 20 to 40 MHz and it has been virtually agreed that the IEEE802.11ac standard will extend the maximum bandwidth from 40 to 80 or 160 MHz [1]. The large number of wireless devices and the increased bandwidth accelerates the shortage of frequency channels and increases ICI. These problems are especially severe in closely spaced residences like apartments in Japan [2].

To improve the system throughput in overlapping cells, references [3]–[9] focused on multi-cell beamforming techniques. These techniques can be divided into two control schemes: centralized [3]–[5] and decentralized [6]–[9]. Although a centralized control scheme can achieve high throughput, all the APs must be synchronized and share all of the transmit data and channel state information (CSI). On the other hand, a decentralized control scheme can also improve the throughput by using the CSI between the AP and user terminal (UT) of its own cell and between the AP and UT of a nearby cell, so the CSI and the transmit data are not shared. Although a decentralized control scheme offers less throughput improvement than a centralized control scheme, it significantly lightens the requirements on the APs. Since the owners of the APs in WLAN systems are generally different, the decentralized control scheme is more suitable for WLAN systems.

Therefore, we consider a multi-cell beamforming technique based on a decentralized control scheme for MIMO-OFDM downlink transmission. Some papers have investigated this type of multi-cell beamforming technique from a theoretical viewpoint [6], [7]. Reference [6] considered multi-cell beamforming based on zero forcing (ZF) under limited backhaul information exchange in cellular systems. Reference [7] considered joint beamforming to mitigate ICI of a primary user in cognitive radio networks. Reference [8] proposed cooperative transmission on the basis of a decentralized control scheme and this scheme attains a high achievable bit rate in an overlapping cell environment through the assumption of a virtual wall. Although the above conventional method improves the system throughput, the signal power is degraded because the degree of freedom (DoF) at the transmitter decreases by nullifying all the antennas at the receiver of the neighboring cell. In addition, [9] investigated the precoding design of interference alignment (IA) which achieves the sum capacity as $C(SNR) = K/2\log(SNR) + o(\log(SNR))$ where SNR is the signal to noise ratio between transmitter and receiver, K is the number of user. Each transmitter using IA transmits data by using transmitter weight based on CSI of all links, thus the amount of CSI is larger than that of [6]–[8] which use part of CSI. Also this precoding design requires phase synchronization among multiple APs, which is not practical for different owner's APs.

In this paper, we propose an interference-aware multi-

Manuscript received August 31, 2012.
Manuscript revised February 5, 2013.

[†]The authors are with NTT Network Innovation Laboratories, NTT Corporation, Yokosuka-shi, 239-0847 Japan.
[††]The author is with the Faculty of Engineering, Iwate University, Morioka-shi, 020-8551 Japan.
a) E-mail: murakami.tomoki@lab.ntt.co.jp

DOI: 10.1587/transcom.E96.B.1492

cell beamforming (IMB) technique. This technique prevents DoF degradation by selecting interference signal space (ISS) so as to allow a small amount of ICI. Since the DoF at the AP increases by reducing the number of nullifying beams, the total achievable rate can be increased. For single-cell environment, [10] has proposed the generalized approach to the block diagonalization (GBD) based on a concept of projecting the inter-user interference to a limited vector space. This paper focuses on multi-cell environment. The proposed technique selects the ISS to prevent the ICI from becoming more than the allowable interference to noise power ratio P. To evaluate the transmission performance of the proposed technique we measured a CSI in an actual apartment environment. We used the measured CSI in closely spaced residences to analyze the ICI conditions in the apartment and clarify the effectiveness of the proposed technique.

This paper is organized as follows. Section 2 introduces the system model. Section 3 describes multi-cell beamforming including the conventional and proposed techniques. Section 4 details our measurement experiment and interference CSI analysis. Section 5 clarifies the effectiveness of the IMB. We conclude with a summary of key points in Sect. 6.

This paper will use the following mathematical notations: $[\cdot]^H$ for Hermitian transposition, det($\mathbf{A}$) for the determinant of $\mathbf{A}$, $\|\mathbf{A}\|_F$ for the Frobenius norm of $\mathbf{A}$, and $\varepsilon\{\mathbf{A}\}$ for expectation of $\mathbf{A}$.

2. System Model

We assume MIMO-OFDM downlink transmission in an overlapping cell environment where two APs utilize the same frequency channel (Fig. 1). This system model indicates one specific subcarrier in all the subcarrier. It is assumed that both APs are equipped with N transmit antennas for communication with their own UTs equipped with M receive antennas ($N \geq M$). $\mathbf{H}_{11(k)}$ and $\mathbf{H}_{22(k)} \in \mathbb{C}^{M\times N}$ denote the CSI of kth ($k = 1, \ldots, K$) subcarrier of a desired signal between AP 1 and UT 1 and between AP 2 and UT 2, respectively. $\mathbf{H}_{12(k)}$ and $\mathbf{H}_{21(k)} \in \mathbb{C}^{M\times N}$ denote the interference CSI of kth subcarrier of an interference signal between AP 1 and UT 2 and between AP 2 and UT 1, respectively. In this paper, we assume that each AP estimates downlink CSI using received signals in uplink transmission by the channel reciprocity in time division duplex (TDD) systems. Thus, each AP obtains CSI corresponding to all UTs which includes the other cell's UTs. In this system model, the received signal vectors of kth subcarrier, $\mathbf{y}_{1(k)} \in \mathbb{C}^{M\times 1}$ at UT 1 and $\mathbf{y}_{2(k)} \in \mathbb{C}^{M\times 1}$ at UT 2, are expressed by the transmit signal vector of kth subcarriers $\mathbf{x}_{1(k)} \in \mathbb{C}^{N_{stm1(k)}\times 1}$ of AP 1 and $\mathbf{x}_{2(k)} \in \mathbb{C}^{N_{stm2(k)}\times 1}$ of AP 2 as

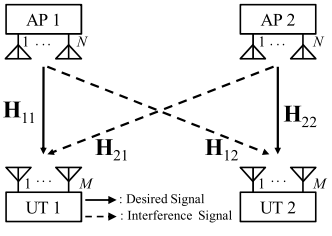

Fig. 1 System model.

$$\begin{cases} \mathbf{y}_{1(k)} = \mathbf{H}_{11(k)}\mathbf{W}_{1(k)}\sqrt{\mathbf{P}_{1(k)}}\mathbf{x}_{1(k)} \\ \qquad +\mathbf{H}_{21(k)}\mathbf{W}_{2(k)}\sqrt{\mathbf{P}_{2(k)}}\mathbf{x}_{2(k)} + \mathbf{n}_{1(k)} \\ \mathbf{y}_{2(k)} = \mathbf{H}_{22(k)}\mathbf{W}_{2(k)}\sqrt{\mathbf{P}_{2(k)}}\mathbf{x}_{2(k)} \\ \qquad +\mathbf{H}_{12(k)}\mathbf{W}_{1(k)}\sqrt{\mathbf{P}_{1(k)}}\mathbf{x}_{1(k)} + \mathbf{n}_{2(k)} \end{cases}, \tag{1}$$

where $N_{stm1(k)}$ and $N_{stm2(k)}$ are the number of streams at the AP 1 and AP 2, and $\mathbf{W}_{1(k)}$ and $\mathbf{W}_{2(k)}$ are the transmission weights of kth subcarrier of AP 1 and AP 2 in calculating CSI including estimation error, respectively. $\mathbf{n}_{1(k)}$ and $\mathbf{n}_{2(k)}$ are additive white Gaussian noise vectors, respectively, with $\mathrm{E}[\mathbf{n}_{1(k)}\mathbf{n}_{1(k)}^H] = \mathrm{E}[\mathbf{n}_{2(k)}\mathbf{n}_{2(k)}^H] = \sigma^2\mathbf{I}$. $\mathbf{I}$ is the identity matrix. $\mathbf{P}_{1(k)} \in \mathbb{C}^{N_{stm1(k)}\times N_{stm1(k)}}$ and $\mathbf{P}_{2(k)} \in \mathbb{C}^{N_{stm2(k)}\times N_{stm2(k)}}$ are diagonal matrices with the diagonal elements of $p_{(k)}/N_{stm1(k)}$ and $p_{(k)}/N_{stm2(k)}$ for the AP 1 and AP 2, respectively. $p_{(k)}$ is transmit power of kth subcarrier. In this paper, since the measurement environment of this paper is high SNR environment, we assumed equal power is allocated to each data stream. This is because the gain of power allocation technique such as water-filling is less at high SNR environment [11].

We assume that CSI at the transmitter includes estimation error due to estimation noise such as thermal noise, quantization error, a reduced amount of feedback information, and time variation of the channel [12]–[14]. The imperfect CSI including the estimation error $\mathbf{H}'_{ij(k)}$ is defined as

$$\mathbf{H}'_{ij(k)} = \mathbf{H}_{ij(k)} + \mathbf{\Delta}_{ij(k)}, \forall i,\ j = 1, 2 \tag{2}$$

where $\mathbf{\Delta}_{ij(k)}$ is assumed to be as all i.i.d. zero-mean complex Gaussian values with the variance of σ_E^2.

3. Multi-Cell Beamforming Techniques

3.1 Conventional Technique

In the conventional technique [8], both APs communicate with their own destination UT and mitigate ICI to the other cell's UT by ZF transmission [15], [16]. The desired signals are transmitted by using eigenvector transmission [17]. Next we explain the transmission weight of each AP and the achievable rate of the conventional technique.

By using singular value decomposition (SVD), the estimated CSI including estimation error as CSI at the transmitter, $\mathbf{H}'_{12(k)}$ and $\mathbf{H}'_{21(k)}$ are expressed as

$$\begin{cases} \mathbf{H}'_{12(k)} = \mathbf{U}_{12(k)}\left(\mathbf{\Sigma}_{12(k)} \quad \mathbf{0}\right)\left(\mathbf{V}^{(s)}_{12(k)} \quad \mathbf{V}^{(n)}_{12(k)}\right)^H \\ \mathbf{H}'_{21(k)} = \mathbf{U}_{21(k)}\left(\mathbf{\Sigma}_{21(k)} \quad \mathbf{0}\right)\left(\mathbf{V}^{(s)}_{21(k)} \quad \mathbf{V}^{(n)}_{21(k)}\right)^H \end{cases}, \tag{3}$$

where $\mathbf{U}_{12(k)}$ and $\mathbf{U}_{21(k)} \in \mathbb{C}^{M\times M}$ are the left singular vectors and $(\mathbf{V}^{(s)}_{12(k)}\ \mathbf{V}^{(n)}_{12(k)})$ and $(\mathbf{V}^{(s)}_{21(k)}\ \mathbf{V}^{(n)}_{21(k)}) \in \mathbb{C}^{N\times N}$ are the right singular vectors. $\mathbf{V}^{(s)}_{12(k)}$, $\mathbf{V}^{(s)}_{21(k)} \in \mathbb{C}^{N\times M}$ and $\mathbf{V}^{(n)}_{21(k)}$,

$\mathbf{V}^{(n)}_{12(k)} \in \mathbb{C}^{N\times(N-M)}$ correspond to signal and null space, respectively. $\mathbf{\Sigma}_{12(k)}$ and $\mathbf{\Sigma}_{21(k)} \in \mathbb{C}^{M\times M}$ are diagonal matrices and the diagonal elements of $\mathbf{\Sigma}_{12(k)}$ and $\mathbf{\Sigma}_{21(k)}$ represent the square roots of the eigenvalues, $\lambda_{12(k),1}, \ldots, \lambda_{12(k),M}$ and $\lambda_{21(k),1}, \ldots, \lambda_{21(k),M}$, respectively, where $\lambda_{ij(k),1} \geq \ldots \geq \lambda_{ij(k),M}$. To calculate the transmission weight, the SVD is performed for the null space CSI, $\mathbf{H}'_{11(k)}\mathbf{V}^{(n)}_{12(k)}$ and $\mathbf{H}'_{22(k)}\mathbf{V}^{(n)}_{21(k)}$, as

$$\begin{cases} \mathbf{H}'_{11(k)}\mathbf{V}^{(n)}_{12(k)} \\ \quad = \left(\bar{\mathbf{U}}^{(s)}_{11(k)} \;\; \bar{\mathbf{U}}^{(n)}_{11(k)}\right)\begin{pmatrix} \bar{\mathbf{\Sigma}}_{11(k)} & \mathbf{0} \\ \mathbf{0} & \mathbf{0} \end{pmatrix}\left(\bar{\mathbf{V}}^{(s)}_{11(k)} \;\; \bar{\mathbf{V}}^{(n)}_{11(k)}\right)^H \\ \mathbf{H}'_{22(k)}\mathbf{V}^{(n)}_{21(k)} \\ \quad = \left(\bar{\mathbf{U}}^{(s)}_{22(k)} \;\; \bar{\mathbf{U}}^{(n)}_{22(k)}\right)\begin{pmatrix} \bar{\mathbf{\Sigma}}_{22(k)} & \mathbf{0} \\ \mathbf{0} & \mathbf{0} \end{pmatrix}\left(\bar{\mathbf{V}}^{(s)}_{22(k)} \;\; \bar{\mathbf{V}}^{(n)}_{22(k)}\right)^H \end{cases}, \quad (4)$$

where $\left(\bar{\mathbf{U}}^{(s)}_{11(k)} \;\; \bar{\mathbf{U}}^{(n)}_{11(k)}\right)$ and $\left(\bar{\mathbf{U}}^{(s)}_{22(k)} \;\; \bar{\mathbf{U}}^{(n)}_{22(k)}\right) \in \mathbb{C}^{M\times M}$ are the left singular vectors and $\left(\bar{\mathbf{V}}^{(s)}_{11(k)} \;\; \bar{\mathbf{V}}^{(n)}_{11(k)}\right)$ and $\left(\bar{\mathbf{V}}^{(s)}_{22(k)} \;\; \bar{\mathbf{V}}^{(n)}_{22(k)}\right)$ $\in \mathbb{C}^{(N-M)\times(N-M)}$ are the right singular vectors. $\bar{\mathbf{V}}^{(s)}_{11(k)}$, $\bar{\mathbf{V}}^{(s)}_{22(k)}$ $\in \mathbb{C}^{N\times N_{stm(k)}}$ and $\bar{\mathbf{V}}^{(n)}_{11(k)}$, $\bar{\mathbf{V}}^{(n)}_{22(k)} \in \mathbb{C}^{N\times(N-M-N_{stm(k)})}$ correspond to signal and null spaces, respectively. Hereafter, the number of data streams, $N_{stm(k)}$ is defined as $\min(M, N-M)$. Thus, conventional multi-cell beamforming cannot be used when the receive antenna number is equal to the transmit antenna number, $N = M$. $\bar{\mathbf{\Sigma}}_{11(k)}$ and $\bar{\mathbf{\Sigma}}_{22(k)}$ are diagonal matrices and the diagonal elements of $\bar{\mathbf{\Sigma}}_{11(k)}$ and $\bar{\mathbf{\Sigma}}_{22(k)}$ represent the square roots of the eigenvalues, $\lambda_{11(k),1}, \ldots, \lambda_{11(k),N_{stm(k)}}$ and $\lambda_{22(k),1}, \ldots, \lambda_{22(k),N_{stm(k)}}$, respectively, where $\lambda_{ii(k),1} \geq \ldots \geq \lambda_{ii(k),N_{stm(k)}}$. Thus, the transmission weights of AP 1 and AP 2, $\mathbf{W}_{a,1(k),}$ and $\mathbf{W}_{a,2(k)}$, are expressed as

$$\begin{cases} \mathbf{W}_{a,1(k)} = \mathbf{V}^{(n)}_{12(k)}\bar{\mathbf{V}}^{(s)}_{11(k)} \\ \mathbf{W}_{a,2(k)} = \mathbf{V}^{(n)}_{21(k)}\bar{\mathbf{V}}^{(s)}_{22(k)} \end{cases}. \quad (5)$$

We next explain the achievable rate of the conventional technique using the transmission weights of AP 1 and AP 2 as expressed in (5). The achievable rates of each cell, $C_{a,1(k)}$ and $C_{a,2(k)}$, are expressed by

$$\begin{cases} C_{a,1(k)} = \log_2 \det\left(\mathbf{I}_{N_{stm(k)}} \right. \\ \quad \left. + \dfrac{\mathbf{H}_{11(k)}\mathbf{W}_{a,1(k)}\mathbf{P}_{1(k)}\mathbf{W}^H_{a,1(k)}\mathbf{H}^H_{11(k)}}{\sigma^2\mathbf{I}_{N_{stm(k)}} + \mathbf{H}_{21(k)}\mathbf{W}_{a,2(k)}\mathbf{P}_{2(k)}\mathbf{W}^H_{a,2(k)}\mathbf{H}^H_{21(k)}}\right). \\ C_{a,2(k)} = \log_2 \det\left(\mathbf{I}_{N_{stm(k)}} \right. \\ \quad \left. + \dfrac{\mathbf{H}_{22(k)}\mathbf{W}_{a,2(k)}\mathbf{P}_{2(k)}\mathbf{W}^H_{a,2(k)}\mathbf{H}^H_{22(k)}}{\sigma^2\mathbf{I}_{N_{stm(k)}} + \mathbf{H}_{12(k)}\mathbf{W}_{a,1(k)}\mathbf{P}_{1(k)}\mathbf{W}^H_{a,1(k)}\mathbf{H}^H_{12(k)}}\right) \end{cases} \quad (6)$$

Moreover, the total achievable rate $C_{a(k)}$ is taken to be the summation of $C_{a,1(k)}$ and $C_{a,2(k)}$. In the conventional technique, ICI is mitigated by nullifying all the ISS by beamforming, but the signal space to the UT is also limited because the DoF at the AP is limited.

3.2 Interference-Aware Multi-Cell Beamforming (IMB)

In this subsection, we introduce an interference-aware multi-cell beamforming (IMB) technique including a method of selecting the ISS. The IMB technique is able to increase the signal space by increasing the number of column vectors of $\mathbf{V}^{(n)}_{12(k)}$ and $\mathbf{V}^{(n)}_{21(k)}$, respectively. To increase the signal space, both APs set a common allowable interference to noise power ratio P in all of the subcarriers and add $S_{1(k)}$ column vectors of $\mathbf{V}^{(s)}_{12(k)}$ and $S_{2(k)}$ column vectors of $\mathbf{V}^{(s)}_{21(k)}$ in each subcarrier, respectively. Here, P is determined by Scheme I in last of this section. Provided that it is necessary that the initial value of P is set as low value in order to maximize the total achievable rate. The added $S_{1(k)}$ and $S_{2(k)}$ are selected to ensure that the corresponding eigenvalues are less than P. This is expressed as

$$\begin{cases} S_{1(\mathrm{k})} = \arg\max\limits_{s} \sum\limits_{i=M-s+1}^{M} \dfrac{\lambda_{12(k),i}}{\sigma^2} \\ \text{subject to} \sum\limits_{i=M-s+1}^{M} \dfrac{\lambda_{12(k),i}}{\sigma^2} < P \\ S_{2(\mathrm{k})} = \arg\max\limits_{s} \sum\limits_{i=M-s+1}^{M} \dfrac{\lambda_{21(k),i}}{\sigma^2} \\ \text{subject to} \sum\limits_{i=M-s+1}^{M} \dfrac{\lambda_{12(k),i}}{\sigma^2} < P \end{cases}, \quad (7)$$

where $\lambda_{12(k),i}$ and $\lambda_{21(k),i}$ are the eigenvalues of $\mathbf{H}^H_{12(k)}\mathbf{H}_{12(k)}$ and $\mathbf{H}^H_{21(k)}\mathbf{H}_{21(k)}$, respectively. The extended null matrices, $\mathbf{V}^{(n)}_{12(k),S} \in \mathbb{C}^{N\times(N-M+S_{1(k)})}$ and $\mathbf{V}^{(n)}_{21(k),S} \in \mathbb{C}^{N\times(N-M+S_{2(k)})}$, are expressed as

$$\begin{cases} \mathbf{V}^{(n)}_{12(\mathrm{k}),S} = \begin{bmatrix} \alpha^{(s)}_{(M-S_{1(k)}+1)1(k)} & \cdots & \alpha^{(s)}_{M1(k)} & \alpha^{(n)}_{11(k)} & \cdots & \alpha^{(n)}_{(N-M)1(k)} \\ \vdots & \ddots & \vdots & \vdots & \ddots & \vdots \\ \alpha^{(s)}_{(M-S_{1(k)}+1)N(k)} & \cdots & \alpha^{(s)}_{MN(k)} & \alpha^{(n)}_{1N(k)} & \cdots & \alpha^{(n)}_{(N-M)N(k)} \end{bmatrix} \\ \mathbf{V}^{(n)}_{21(\mathrm{k}),S} = \begin{bmatrix} \beta^{(s)}_{(M-S_{2(k)}+1)1(k)} & \cdots & \beta^{(s)}_{M1(k)} & \beta^{(n)}_{11(k)} & \cdots & \beta^{(n)}_{(N-M)1(k)} \\ \vdots & \ddots & \vdots & \vdots & \ddots & \vdots \\ \beta^{(s)}_{(M-S_{2(k)}+1)N(k)} & \cdots & \beta^{(s)}_{MN(k)} & \beta^{(n)}_{1N(k)} & \cdots & \beta^{(n)}_{(N-M)N(k)} \end{bmatrix} \end{cases}, \quad (8)$$

where $\alpha^{(s)}_{ij(k)}$ and $\alpha^{(n)}_{ij(k)}$ are elements in the i-th row and j-th column of $\mathbf{V}^{(s)}_{12(k)}$ and $\mathbf{V}^{(n)}_{12(k)}$, $\beta^{(s)}_{ij(k)}$ and $\beta^{(n)}_{ij(k)}$ are elements in the i-th row and j-th column of $\mathbf{V}^{(s)}_{21(k)}$ and $\mathbf{V}^{(n)}_{21(k)}$. The SVD is carried out for $\mathbf{H}'_{11(k)}\mathbf{V}^{(n)}_{12(k),S}$ and $\mathbf{H}'_{22(k)}\mathbf{V}^{(n)}_{21(k),S}$ as

$$\begin{cases} \mathbf{H}'_{11(k)}\mathbf{V}^{(n)}_{12(k),S} \\ \quad = \left(\bar{\mathbf{U}}^{(s)}_{11(k),S} \;\; \bar{\mathbf{U}}^{(n)}_{11(k),S}\right)\begin{pmatrix} \bar{\mathbf{\Sigma}}_{11(k),S} & \mathbf{0} \\ \mathbf{0} & \mathbf{0} \end{pmatrix}\left(\bar{\mathbf{V}}^{(s)}_{11(k),S} \;\; \bar{\mathbf{V}}^{(n)}_{11(k),S}\right)^H \\ \mathbf{H}'_{22(k)}\mathbf{V}^{(n)}_{21(k),S} \\ \quad = \left(\bar{\mathbf{U}}^{(s)}_{22(k),S} \;\; \bar{\mathbf{U}}^{(n)}_{22(k),S}\right)\begin{pmatrix} \bar{\mathbf{\Sigma}}_{22(k),S} & \mathbf{0} \\ \mathbf{0} & \mathbf{0} \end{pmatrix}\left(\bar{\mathbf{V}}^{(s)}_{22(k),S} \;\; \bar{\mathbf{V}}^{(n)}_{22(k),S}\right)^H \end{cases}. \quad (9)$$

where $\left(\bar{\mathbf{U}}^{(s)}_{11(k),S}\ \bar{\mathbf{U}}^{(n)}_{11(k),S}\right)$ and $\left(\bar{\mathbf{U}}^{(s)}_{22(k),S}\ \bar{\mathbf{U}}^{(n)}_{22(k),S}\right) \in \mathbb{C}^{M\times M}$ are the left singular vectors and $\left(\bar{\mathbf{V}}^{(s)}_{11(k),S}\ \bar{\mathbf{V}}^{(n)}_{11(k),S}\right) \in \mathbb{C}^{(N-M+S_{1(k)})\times(N-M+S_{1(k)})}$ and $\left(\bar{\mathbf{V}}^{(s)}_{22(k),S}\ \bar{\mathbf{V}}^{(n)}_{22(k),S}\right) \in \mathbb{C}^{(N-M+S_{2(k)})\times(N-M+S_{2(k)})}$ are the right singular vectors. $\bar{\mathbf{V}}^{(s)}_{11(k),S} \in \mathbb{C}^{N\times N_{stm1(k)}}$, $\bar{\mathbf{V}}^{(s)}_{22(k),S} \in \mathbb{C}^{N\times N_{stm2(k)}}$ and $\bar{\mathbf{V}}^{(n)}_{11(k),S} \in \mathbb{C}^{N\times(N-M+S\,1(k)-N_{stm1(k)})}$, $\bar{\mathbf{V}}^{(n)}_{22(k),S} \in \mathbb{C}^{N\times(N-M+S\,2(k)-N_{stm2(k)})}$ correspond to signal and null space, respectively. The numbers of data streams for UT 1 and UT 2, $N_{stm1(k)}$ and $N_{stm2(k)}$, are expressed as $\min(M, N-M+S_{1(k)})$ and $\min(M, N-M+S_{2(k)})$, respectively. Since the number of each AP's streams in the IMB technique is adaptively determined by P, the number of nullified interference signal spaces (ISS), $S_{1(k)}$ and $S_{2(k)}$ are optimized for each subcarrier in OFDM systems. Thus, the transmission weights of AP 1 and AP 2, $\mathbf{W}_{b,1}$, and $\mathbf{W}_{b,2}$, are expressed as

$$\begin{cases} \mathbf{W}_{b,1(k)} = \mathbf{V}^{(n)}_{12(k),S}\bar{\mathbf{V}}^{(s)}_{11(k),S} \\ \mathbf{W}_{b,2(k)} = \mathbf{V}^{(n)}_{21(k),S}\bar{\mathbf{V}}^{(s)}_{22(k),S} \end{cases}, \tag{10}$$

Next, we explain the achievable rate of the IMB technique using transmission weights of AP 1 and AP 2 as expressed in (10). The achievable rates between AP 1 and UT 1 and between AP 2 and UT 2, $C_{b,1(k)}$ and $C_{b,2(k)}$, are calculated by

$$\begin{cases} C_{b,1(k)} = \log_2 \det\left(\mathbf{I}_{N_{stm1(k)}} + \dfrac{\mathbf{H}_{11(k)}\mathbf{W}_{b,1(k)}\mathbf{P}_{1(k)}\mathbf{W}^H_{b,1(k)}\mathbf{H}^H_{11(k)}}{\sigma^2\mathbf{I}_{N_{stm1(k)}} + \mathbf{H}_{21(k)}\mathbf{W}_{b,2(k)}\mathbf{P}_{2(k)}\mathbf{W}^H_{b,2(k)}\mathbf{H}^H_{21(k)}}\right) \\ C_{b,2(k)} = \log_2 \det\left(\mathbf{I}_{N_{stm2(k)}} + \dfrac{\mathbf{H}_{22(k)}\mathbf{W}_{b,2(k)}\mathbf{P}_{2(k)}\mathbf{W}^H_{b,2(k)}\mathbf{H}^H_{22(k)}}{\sigma^2\mathbf{I}_{N_{stm2(k)}} + \mathbf{H}_{12(k)}\mathbf{W}_{b,1(k)}\mathbf{P}_{1(k)}\mathbf{W}^H_{b,1(k)}\mathbf{H}^H_{12(k)}}\right) \end{cases} \tag{11}$$

Moreover, the total achievable rate of the optimal selection method for the IMB technique, $C_{b(k)}$, is expressed by the summation of $C_{b,1(k)}$ and $C_{b,2(k)}$.

We next describe the transmission scheme of each AP including the setting method of an allowable interference to noise power ratio P in Scheme I. In this scheme, P_0 [dB] is the initial value of P and is set up a low value such as the noise power. ΔP [dB] is the value for updating of P and is set up several decibels. C_m [bit/s/Hz] is the rate-update margin against the rate deviation caused by noise and is set up several bits/s/Hz.

Scheme I: The transmission scheme for the IMB technique

1): Initialization: $P = P_0$, $C_{b,0} = 0$
2): Repeat
  2a): Select $S_{1(k)}$ or $S_{2(k)}$ by (7)
  2b): Transmit data using transmission weight in (10)
  2c): Calculate $C_{b,1(k)}$ and $C_{b,2(k)}$ in (11) for all subcarriers at UT 1 and UT 2, respectively
  2d): Feed the information of the averaged achievable rate for all the subcarriers, $\sum_{k=1}^{K} C_{b,1(k)}/K$ and $\sum_{k=1}^{K} C_{b,2(k)}/K$, back to both APs and calculate the total achievable rate C'_b that is the summation of $\sum_{k=1}^{K} C_{b,1(k)}/K$ and $\sum_{k=1}^{K} C_{b,2(k)}/K$
  2e): if $C'_b - C_{b,0} \geq -C_m$
    Update$P = P+\Delta P$, $C_{b,0} = C'_b$
  else
    End

4. CSI Measurement Experiment

4.1 Experiment Setup

To evaluate the effectiveness of the IMB technique, we measured the CSI for OFDM systems in an actual apartment using a MIMO-OFDM testbed. Figure 2 shows an apartment in Japan. The height, width and depth of the room are 3, 3, and 4.4 m, respectively. We conducted the experiments in rooms 1-5. The configuration of our MIMO-OFDM transceivers [18] is shown in Fig. 3. Its main parameters per room are given in Table 1. The MIMO-OFDM transceivers transmit the pilot signal based on short and long

Fig. 2 Photograph of measured apartment.

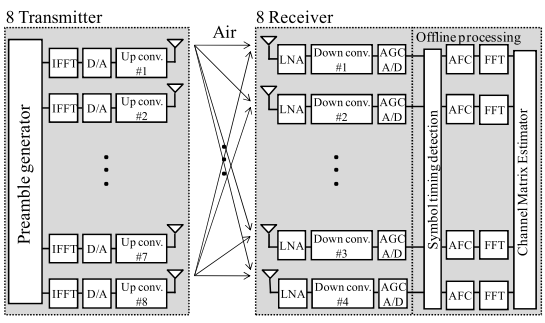

Fig. 3 Configuration of MIMO-OFDM measurement testbed.

Table 1 Measurement parameters per room.

Number of antennas	8 (Tx), 8 (Rx)
Center frequency	4.85 GHz
Bandwidth	20 MHz
Number of FFT points	64
Number of subcarriers, k	52
Interval of subcarriers	312.5kHz
Element spacing	0.5 λ
Antenna height	0.9 m
Tx antenna position	1
Rx antenna position	4
Total transmmission power	9 dBm
Noise power per subcarrier	-113.26 dBm

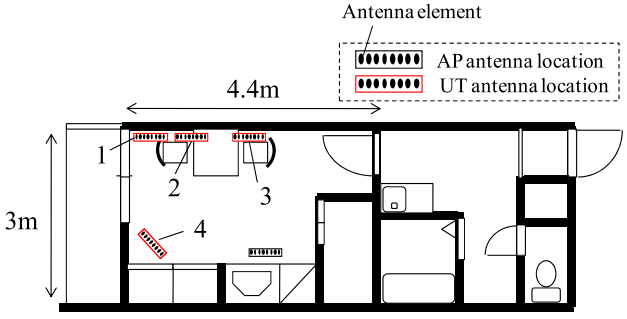

Fig. 4 Room layout, measurement locations.

Fig. 5 Photographs of AP antenna (a) and UT antenna (b).

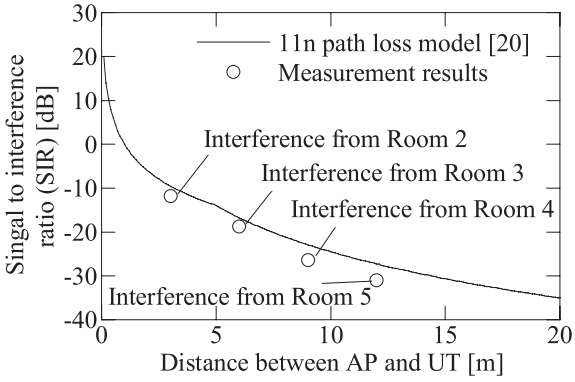

Fig. 6 Ratio of the signal power from AP in Room 1 to the interference power from AP in other rooms at UTs in Room1.

preambles of the IEEE802.11n standard. Thus, the CSI for the 52 subcarriers were estimated in 20 MHz bandwidth. Noise power per subcarrier was −113.26 dBm.

In the experiment, we measured 8 × 8 MIMO-OFDM CSI between the AP and UTs in a single room and between different rooms by using our MIMO-OFDM transceivers [18]. In this paper, since we assume that the proposed technique applies to WLAN systems, we use eight transmitter and eight receiver antennas. This is because the maximum antenna number in IEEE802.11ac [2] is eight. Figure 4 indicates the room layout and the locations of the AP and UTs. UTs are set four locations in order to evaluate difference environments such as multipath and fading. The AP and UT antennas had uniform linear array (ULA) with eight element dipole antennas and element spacing of 0.5 wavelengths. Figures 5(a) and 5(b) show the AP and UT antennas we used. Both antennas are 0.9 m high. The total transmission power of each AP is 9 dBm.

4.2 Interference CSI Analysis

In this subsection, we analyze the amount of ICI and the eigenvalue distribution of interference CSI, $\mathbf{H}_{12(k)}$, which correspond to the CSI between the AP in Room 1 and UTs in Room 2, 3, 4, and 5, and $\mathbf{H}_{21(k)}$, which correspond to the CSI between APs in Room 2/3/4/5 and UTs in Room 1.

Figure 6 plots the ratio of the signal power from AP in Room 1 to the interference power from AP in other rooms at UTs in Room1. Plots of the signal to interference ratio (SIR) is calculated by,

$$SIR = \frac{\varepsilon\left\{P_{1(k)}\left\|\mathbf{H}_{11(k,l)}\right\|_F^2\right\}}{\varepsilon\left\{P_{2(k)}\left\|\mathbf{H}_{21(k,l)}\right\|_F^2\right\}}, \quad \begin{cases} k = 1, \cdots 52 \\ l = 1, \cdots 4 \end{cases}, \qquad (12)$$

where $\mathbf{H}_{21(k,l)}$ is the CSI between AP in other rooms and lth UT in Room 1. The SIRs calculated by (12) are plotted at the distance of each AP position and the center of Room 1. This figure also shows the theoretical line according to the indoor propagation model described in IEEE802.11n [19]. In this theoretical line, we assumed that wall loss value is 0 dB and signal power is received power when distance AP and UT is 1 m. In this apartment, the walls were made of plaster board that had low propagation loss because of low permittivity [20]. We found that SIR is about −30 dB when the AP and UT are set in Rooms 1 and 5. Therefore, we can see that the AP incurs severe ICI in this environment.

Figure 7(a) shows the cumulative distribution functions (CDFs) of eigenvalues for i.i.d. channel matrices when the total power is 0 dBm. It was found that the ratio of the highest eigenvalue, λ_1, to the lowest eigenvalue, λ_8, on median value is 25 dB. Figures 7(b)–(e) show the CDFs of eigenvalues for the measured interference CSI, $\mathbf{H}_{12(k,l)}$ and $\mathbf{H}_{21(k,l)}$, of the four points of the UT and the 52 subcarriers. To ensure that the fading among subcarriers would not affect the distributions of eigenvalues, the Frobenius norm of the CSI

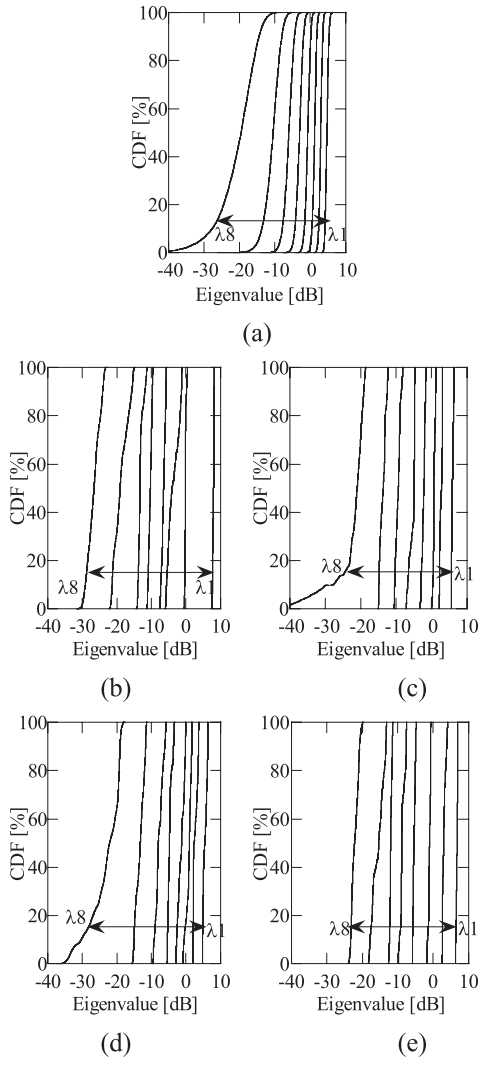

Fig. 7 CDF of eigenvalues of interference CSI. (a) is eigenvalues of i.i.d. channel, (b) is eigenvalues of interference CSI when the UTs are set in Room 2, (c) for Room 3, (d) for Room 4, and (e) for Room 5.

at each subcarrier was normalized to be 0 dB. We found that the ratios between λ_1 and λ_8 medium values were about 38, 25, 26, and 27 dB. The ratio between λ_1 and λ_8 in Room 2 was larger than that of the i.i.d. channel. This is because the effect of the direct path is larger than that of other paths when the distance between the AP and the UT is short.

5. Performance Evaluation

In this section, we evaluate the effectiveness of the IMB technique using measured CSI. We assumed that AP 1 and AP 2 were located in two different rooms, i.e., Rooms 1 and 2, 1 and 3, 1 and 4, and 1 and 5 (hereafter Rooms 1-2, Rooms 1-3, Rooms 1-4, and Rooms 1-5, respectively). Moreover, we also assume that both of APs transmit data UTs in own room.

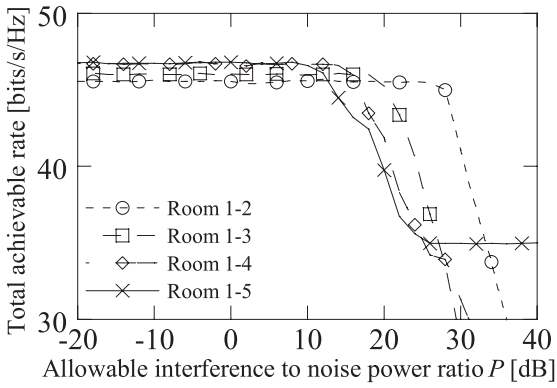

Fig. 8 M = 2 total achievable rate vs. allowable interference to noise power ratio P.

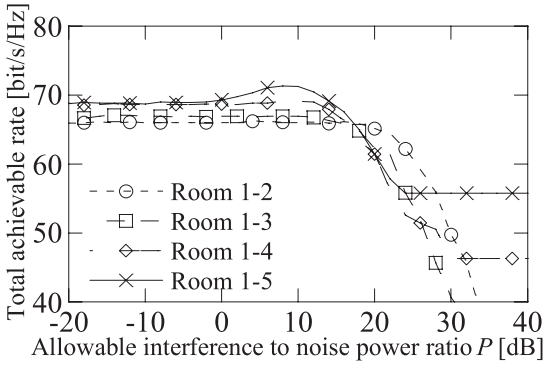

Fig. 9 M = 4 total achievable rate vs. allowable interference to noise power ratio P.

5.1 Allowable Interference to Noise Power Ratio P Analysis

In this subsection, we show a study of allowable interference to noise power ratio P when the number of UT antennas M is 2, 4, 6, and 8. Figures 8, 9, 10, and 11 show the total achievable rate that averages the four points of UT and all subcarriers versus the allowable interference to noise power ratio P when the number of UT antennas M is 2, 4, 6, and 8, respectively. In Fig. 8 (M = 2), we found that the total achievable rates of all the room combinations degrades when P becomes larger. Since the number of UT antennas is small, the gain obtained by increasing the DoF at the AP using the extended null matrix is negligible. Furthermore, the total achievable rate maximizes when $S_{1(k)}$ and $S_{2(k)}$ are set to 0 in almost all subcarriers since the smallest eigenvalue is very large.

In Fig. 9 (M = 4), the results obtained for Rooms 1-2 and 1-3 are similar to those in Fig. 8. This is also because the gain obtained by increasing the DoF at the AP is less than the loss incurred by increasing the ICI. However, the results obtained for Room 1-4 and 1-5 show local maxima. The local maximum values of P of Rooms 1-4 and 1-5 are 10 and 8 dB, respectively. These local maxima show that the proposed technique increases the total achievable rate

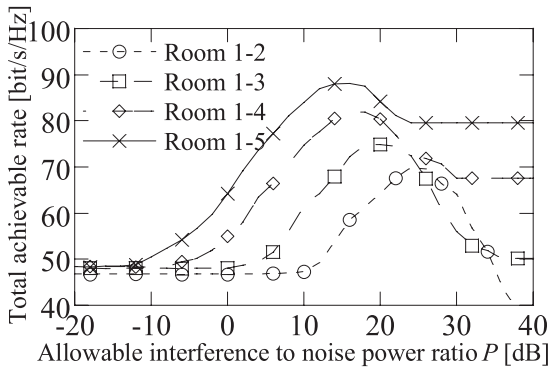

Fig. 10 $M = 6$ total achievable rate vs. allowable interference to noise power ratio P.

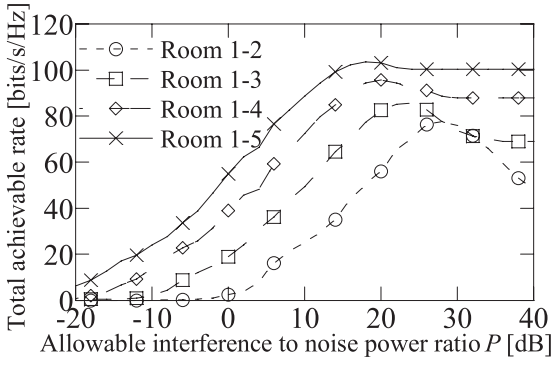

Fig. 11 $M = 8$ total achievable rate vs. allowable interference to noise power ratio P.

by increasing the number of column vectors of $\mathrm{V}_{ij(k)}^{(n)}$.

In Fig. 10 ($M = 6$), we find that a local maximum exists in all the results. Since the lower eigenvalues decrease due to the increased number of eigenvalues of the interference CSI, the effectiveness of the IMB technique improves. The local maximum value of P is 24 dB for Rooms 1-2, 20 dB for Rooms 1-3, 18 dB for Rooms 1-4, and 16 dB for Rooms 1-5. Moreover, we confirmed that the local maximum peak shifts as the distance between cells becomes longer. This is because the gain obtained using an extended null matrix becomes larger as the distance between cells becomes greater.

In Fig. 11 ($M = 8$), a local maximum also exists in all cases. The local maximum value of P is 28 dB for Rooms 1-2, 24 dB for Rooms 1-3, 20 dB for Rooms 1-4, and 18 dB for Rooms 1-5. We found that the peak of the results in Fig. 10 and Fig. 11 are different. This means that the peak also changes according to the number of UT antennas a nearby cell uses. Note that none of the total achievable rates have local minimum values. Thus, P can be determined by using the transmission scheme shown in Scheme I since the scheme gradually increases P so as not to decrease the total achievable rate.

Table 2 shows the allowable interference to noise power ratio, P [dB], calculated by Scheme I and the maximum value, P_{max} [dB] of P estimated from Fig. 8 ~ Fig. 11. P_{max} means the value of P which maximizes total achievable rate. In this result, we assume that P_0, ΔP_0, and C_m are −20 dB, 2 dB, and 0.5 bit/s/Hz, respectively. From this result of P and P_{max} in Table 2, we found that P is able to be calculated in the accuracy of less than 2 dB by using Scheme I.

Table 2 Allowable interference to noise power ratio, P [dB], calculated by Scheme I and maximum value, P_{max} [dB], of P estimated from Fig. 8 ~ Fig. 11.

	Number of UT antennas, M			
	2	4	6	8
Room 1-2	$P = 26$ $P_{max} = 24$	$P = 16$ $P_{max} = 16$	$P = 24$ $P_{max} = 24$	$P = 28$ $P_{max} = 28$
Room 1-3	$P = 18$ $P_{max} = 17$	$P = 6$ $P_{max} = 6$	$P = 20$ $P_{max} = 20$	$P = 24$ $P_{max} = 24$
Room 1-4	$P = 14$ $P_{max} = 12$	$P = 12$ $P_{max} = 10$	$P = 18$ $P_{max} = 18$	$P = 20$ $P_{max} = 20$
Room 1-5	$P = 10$ $P_{max} = 8$	$P = 10$ $P_{max} = 8$	$P = 16$ $P_{max} = 16$	$P = 18$ $P_{max} = 18$

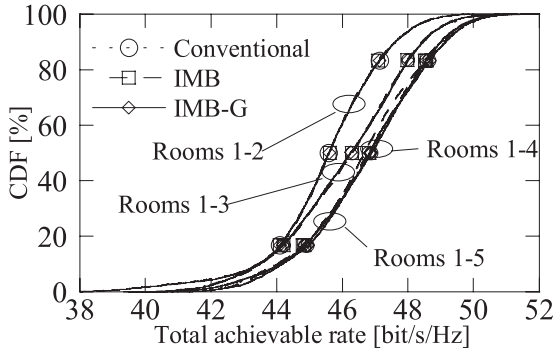

Fig. 12 CDF of $M = 2$ total achievable rate.

5.2 Total Achievable Rate Analysis

In this subsection, to evaluate the transmission scheme in Scheme I, we calculate the total achievable rate of the IMB technique where $S_{1(k)}$ and $S_{2(k)}$ are optimized by a greedy algorithm [21] for purposes of comparison. The IMB technique based on the greedy algorithm is expressed as IMB-G. The calculation complexity of IMB-G is extremely large since the achievable rates must be calculated for all combinations of $S_{1(k)}$ and $S_{2(k)}$. Figures 12, 13, 14, and 15 show the CDFs with the four points of UT and all subcarriers of total achievable rates of the IMB technique, IMB-G, and the conventional technique when the number of UT antennas M is 2, 4, 6, and 8, respectively.

In Fig. 12, allowable interference to noise ratio P of Room 1-2, Room 1-3, Room 1-4, and Room 1-5 are set 26, 18, 14, and 10 [dB], respectively. The total achievable rates of all the results are the same for all room combinations. This indicates that the IMB technique's effectiveness is negligible when the number of UT antennas is small.

In Fig. 13, allowable interference to noise ratio P of Room 1-2, Room 1-3, Room 1-4, and Room 1-5 are set 16, 6, 12, and 10 [dB], respectively. The total achievable rates of all the results are almost the same in Rooms 1-2 and 1-3.

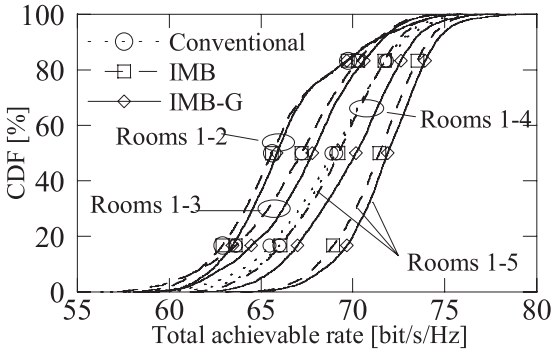

Fig. 13 CDF of $M = 4$ total achievable rate.

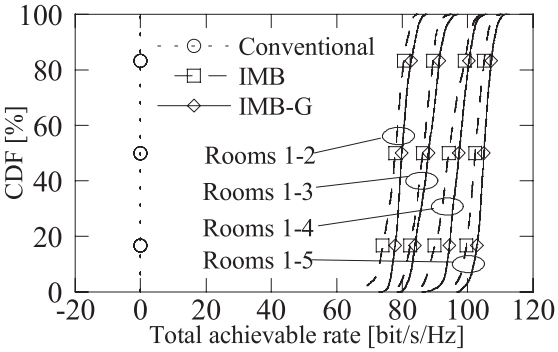

Fig. 15 CDF of $M = 8$ total achievable rate.

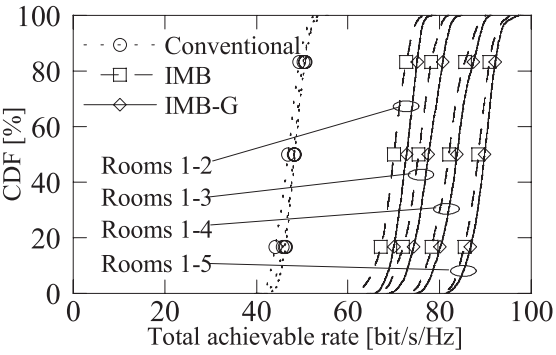

Fig. 14 CDF of $M = 6$ total achievable rate.

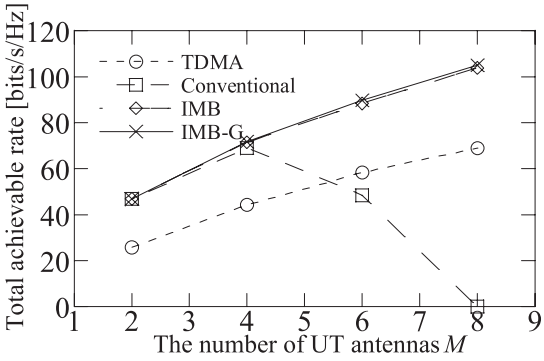

Fig. 16 Total achievable rate vs. number of UT antennas M.

However, in Room 1-4 and 1-5, the median total achievable rates of the IMB technique are about 0.6 and 2.3 bit/s/Hz higher than those of the conventional technique, respectively. Moreover, the IMB technique almost matches the performance of IMB-G. The median total achievable rates of the IMB technique in Rooms 1-4 and 1-5 are about 0.7 and 0.5 bit/s/Hz lower than those of IMB-G, respectively.

In Fig. 14, allowable interference to noise ratio P of Room 1-2, Room 1-3, Room 1-4, and Room 1-5 are set 24, 20, 18, and 16 [dB], respectively. The IMB technique's total achievable rate increases greatly compared with the conventional technique in all the room combinations. In the conventional technique, since a large number of DoFs at the AP is used to nullify the ISS, the total achievable rate is low. The median total achievable rates of the IMB technique in each room combination increases about 23.1, 27.1, 33.6, and 39.8 bit/s/Hz higher than that of the conventional technique, respectively. Moreover, the median total achievable rates of the IMB technique in each room combination is about 2.6, 2.4, 1.7, and 1.3 bit/s/Hz lower than those of IMB-G, respectively.

In Fig. 15, allowable interference to noise ratio P of Room 1-2, Room 1-3, Room 1-4, and Room 1-5 are set 28, 24, 20, and 18 [dB], respectively. The IMB technique's total achievable rate also increases greatly compared with the conventional technique in all the room combinations. In the conventional technique, the total achievable rate is zero because all the DoFs at the AP are used to nullify the ISS. The IMB technique's median total achievable rate in each room combination increases by about 77.4, 86.0, 94.4, and 102.2 bit/s/Hz, respectively, compared with the conventional technique. Moreover, the IMB technique's median achievable rate in Rooms 1-2, 1-3, 1-4 and 1-5 is about 2.8, 1.9, 2.9 and 2.8 bit/s/Hz lower than those of IMB-G, respectively.

Figure 16 shows the median total achievable rate including the four points of UT and all subcarriers in the IMB technique, the IMB-G, the conventional technique, and TDMA versus the number of UT antennas for the cell relation for Rooms 1-5 only. And allowable interference to noise ratio P is 8, 8, 16, and 18, respectively when M is 2, 4, 6, and 8. In TDMA, the transmissions of AP 1 and AP 2 are divided by time slots and each AP uses eigenvector transmission. In the TDMA results, total achievable rate increases as the number of UT antennas increases. The median total achievable rate of the IMB technique is similar to that of the conventional technique when the number of UT antennas is four or less. However, the median total achievable rate of the IMB technique is larger than that of the conventional technique when the number of UT antennas is more than four. This demonstrates that the IMB technique's effectiveness increases when there are a large number of UT antennas.

6. Conclusion and Future Work

We proposed an interference-aware multi-cell beamforming (IMB) technique on a decentralized control scheme for an overlapping cell environment. Although the conventional

technique based on a decentralized control scheme degrades the signal power at the UT by nullifying all the interference signal spaces (ISS), the IMB technique increases the signal power at the UT by selecting the ISS by allowing a small amount of inter-cell interference (ICI). The proposed technique selects the ISS so as to prevent the ICI from becoming higher than the allowable interference to noise power ratio P at each AP. We analyzed the interference CSI conditions and evaluated the transmission performance of the proposed technique by using a measured CSI in an actual indoor environment. The results demonstrated that the IMB technique becomes more effective as the number of UT antennas in nearby cells increases.

Although the IMB technique is proposed for two APs in overlapping cell, it is applicable for more than two APs by selecting a pair of APs. The effectiveness of IMB technique for more than two APs scenario needs to be evaluated in future work.

Acknowledgments

The authors thank Mr. Kazuyasu Okada of NTT Network Innovation Laboratories for his constant encouragement. They also thank Mr. Yoshinobu Makise, Mr. Masaaki Ida, and Mr. Makoto Yoshikawa of NTT Advanced Technology Corporation for their support.

References

[1] Y. Takatori, K. Nishimori, and S. Kitawaza, "OBSS issue in 802.11ac," IEEE802.11-09/0536r0, May 2009.
[2] R. Stacey, et al., "Specification Framework for TGac," IEEE802.11-09/0992r18, Sept. 2010.
[3] Z. Shen, J.G. Andrews, and B.L. Evans, "Adaptive resource allocation in multiuser OFDM systems with proportional rate constraints," IEEE Trans. Wireless Commun., vol.4, no.6, pp.2726–2737, Nov. 2005.
[4] H. Zhang and H. Dai, "Cochannel interference mitigation and cooperative processing in downlink multicell multiuser MIMO networks," EURASIP Journal on Wireless Communications Networking, vol.2004, no.2, pp.222–235, Dec. 2004.
[5] Y. Takatori, K. Cho, and T. Hori, "New beam-forming algorithm controlling pattern of multiple smart antenna for cellular systems," Proc. IEEE-APS Conference on Antenna and Propagation for Wireless Communications, pp.175–178, Nov. 2000.
[6] A. Tolli, H. Pennanen, and P. Komulainen, "Distributed implementation of coordinated multi-cell beamforming," Proc. IEEE 20th International Symposium on Personal, Indoor and Mobile Radio Communications, pp.818–822, Sept. 2009.
[7] K. Hamdi, W. Zhang, and K.B. Letaief, "Joint beamforming and scheduling in cognitive radio networks," Proc. IEEE Global Telecommunications Conference, pp.2977–2981, Nov. 2007.
[8] R. Kudo, Y. Takatori, K. Nishimori, T. Ichikawa, T. Murakami, M. Mizoguchi, and M. Morikura, "Spatial domain resource sharing for overlapping cells in indoor environment," International Journal of Digital Multimedia Broadcasting, vol.2010, Article ID 642542, 2010.
[9] Hui Shen, Bin Li, and Yi Luo, "Precoding design using interference alignment for the network MIMO," Proc. IEEE 20th International Symposium on Personal, Indoor and Mobile Radio Communications, pp.2519–2523, Sept. 2009.
[10] T. Sada, J. Webber, T. Nishimura, T. Ohane, and Y. Ogawa, "A generalized approach to block diagonalization for multiuser MIMO downlink," Proc. IEEE 20th International Symposium on Personal, Indoor and Mobile Radio Communications, pp.503–508, Sept. 2010.
[11] Z. Shen, R.W. Heath, Jr., J.G. Andrews, and B.L. Evans, "Comparison of space-time water-filling and spatial water-filling for MIMO fading channels," Proc. IEEE Global Telecommunications Conference, pp.431–435, Dec. 2004.
[12] A. Pascual-Iserte, D.P. Palomar, A.I. Perez-Neira, and M.A. Lagunas, "A robust maximin approach for MIMO communications with imperfect channel state information based on convex optimization," IEEE Trans. Signal Process., vol.54, no.1, pp.346–360, Jan. 2006.
[13] A. Kuhne and A. Klein, "Adaptive subcarrier allocation with imperfect channel knowledge versus diversity techniques in a multiuser OFDM system," Proc. IEEE 20th International Symposium on Personal, Indoor and Mobile Radio Communications, pp.1–5, Sept. 2007.
[14] Y. Chen and C. Tellambura, "Performance analysis of maximum ratio transmission with imperfect channel estimation," IEEE Commun. Lett., vol.9, no.4, pp.322–324, April 2005.
[15] T. Yoo and A. Goldsmith, "On the optimal of multiantenna broadcast scheduling using zero-forcing beamforming," IEEE J. Sel. Areas Commun., vol.24, no.3, pp.528–541, March 2006.
[16] Q.H. Spencer, A.L. Swindlehurst, and M. Haardt, "Zero-forcing methods for downlink spatial multiplexing in multi-user MIMO channels," IEEE Trans. Signal Process., vol.52, no.2, pp.461–471, Feb. 2004.
[17] A. Paulraj, R. Nabar, and D. Gore, Introduction to Space-Time Wireless Communications, Cambridge University Press, Cambridge, UK, 2003.
[18] K. Nishimori, R. Kudo, N. Honma, Y. Takatori, and M. Mizoguchi, "16×16 Multiuser MIMO testbed employing simple adaptive modulation scheme," Proc. IEEE 69th Vehicular Technology Conference, pp.1–5, April 2009.
[19] G. Smith, "Overlapping BSS analysis of channel requirements," IEEE802.11-08/1470-04-00aa, May 2009.
[20] Y. Pinhasai, A. Yahalom, and S. Petnev, "Propagation of ultra wideband signals in lossy dispersive media," Proc. IEEE International Conference on Microwaves, Communications, Antennas, and Electronics Systems, pp.1–10, May 2008.
[21] G. Dimic and N.D. Sidiropoulos, "On downlink beamforming with greedy user selection: Performance analysis and a simple new algorithm," IEEE Trans. Signal Process., vol.53, no.10, pp.3857–3868, Oct. 2005.

Tomoki Murakami received B.E. and M.E. degrees from Waseda University, Japan in 2006 and 2008, respectively. In 2008, he joined Nippon Telegraph and Telephone Corporation (NTT) Network Innovation Laboratories, Yokosuka, Japan. His current research interests include multiuser MIMO systems and resource allocation. He received the Young Researcher's Award from IEICE in 2010. He is a member of IEEE.

Riichi Kudo received the B.S. and M.S. degree in geophysics from Tohoku University, Japan, in 2001 and 2003, respectively. He received the Ph.D. degree in informatics from Kyoto university in 2010. In 2003, he joined NTT Network Innovation Laboratories, Yokosuka, Japan. He has been engaged in the MIMO communication systems and the beamforming method. He received the Young Engineer Award from IEICE in 2006, IEEE AP-S Japan Chapter Young Engineer Award in 2010, and the Best Paper Award from IEICE in 2011. His current research interest is multiuser MIMO techniques for wireless LAN systems. He is a member of IEEE.

Takeo Ichikawa received the M.E. degree from Waseda University, Tokyo, Japan, in 1993. Since joining Nippon Telegraph and Telephone (NTT) Corporation in 1993, he has participated in the research and development of PHS-based packet systems and high-speed wireless LAN systems. He received the Young Researcher's Award from IEICE in 1999. Currently, he is a senior research engineer, supervisor at NTT Network Innovation Laboratories, NTT Corporation. He is a member of IEEE.

Naoki Honma received the B.E., M.E., and Ph.D. degrees in electrical engineering from Tohoku University, Sendai, Japan in 1996, 1998, and 2005, respectively. In 1998, he joined the NTT Radio Communication Systems Laboratories, Nippon Telegraph and Telephone Corporation (NTT), in Japan. He is now working for Iwate University. He received the Young Engineers Award from the IEICE of Japan in 2003, the APMC Best Paper Award in 2003, and the Best Paper Award of IEICE Communication Society in 2006, respectively. His current research interest is planar antennas for high-speed wireless communication systems. He is a member of IEEE.

Masato Mizoguchi received the B.E. and M.E. degrees in electrical engineering from Tokyo University of Science, Japan in 1989 and 1991, respectively. In 1991, he joined Nippon Telegraph and Telephone Corporation (NTT) and was mainly engaged in research and development of personal communication systems and high data rate wireless LANs including the IEEE 802.11a systems. He is currently a Senior Research Engineer, Supervisor in the department of Wireless Systems Innovation Laboratory of NTT Network Innovation Laboratories, and is working on research and development of next generation wireless home network. He received the Young Researcher's Award in 1998, the Best Paper Award in 2000 and the Achievement Award in 2006 from IEICE. He is a member of IEEE.